Ionics (2010) 16:61–66
DOI 10.1007/s11581-009-0342-4

ORIGINAL PAPER

Synthesis of macroporous $LiMn_2O_4$ with avian egg membrane as a template

T. Sri Devi Kumari · T. Prem Kumar

Received: 23 October 2008 / Revised: 8 March 2009 / Accepted: 29 March 2009 / Published online: 8 May 2009

Abstract Avian eggshell membrane as a template for the synthesis of a macroporous network of crystalline $LiMn_2O_4$ is demonstrated. Well-formed crystals of average size 600 nm formed a network structure whose average pore size was 2–4 μm. The unique porous structure should make it an attractive cathode material for lithium-ion batteries. In fact, for an 80% cutoff in capacity retention, $LiMn_2O_4$ obtained by a 10-h calcination at 800°C sustained 83 cycles.

Keywords Ceramics · Eggshell membrane · Template · Lithium-ion batteries · Electrochemical properties

Introduction

Methods for the preparation of ceramics with specific chemical compositions and tailored microstructures are constantly being developed in response to increasing number of potential applications in diverse areas including catalysis, energy storage, tissue engineering, etc. Macroporous ceramics (i.e., pore size>50 nm) combine the advantages of diffusion pathways and the high surface areas in such networks [1, 2]. Macroporous ceramics can be prepared by a number of methods such as replica method, sacrificial template method, and direct foaming method [3, 4]. The replica method involves the impregnation of a cellular structure with a suspension of a ceramic or its precursor and subsequent drying and removal of the templating phase to produce a ceramic form which is a positive replica of the template. Many synthetic and natural cellular structures can be used as templates to fabricate macroporous ceramics through the replica technique. In the sacrificial template method, a biphasic composite of ceramic particles or their precursors and a sacrificial phase is made from which the latter is extracted to generate porous materials that are a negative replica of the original sacrificial template. In the direct foaming method, air is incorporated into a suspension or liquid media, which is subsequently set in order to retain the structure of air bubbles created as consolidated foams, which are sintered to yield porous ceramics.

Macroporous networks have been synthesized using synthetic templates such as polyurethane foams [5] as well as natural templates such as wood cellular structures [6], starch gels [2], and even organized bacterial threads [1]. Naturally occurring cellular structures are particularly interesting as templates, due mainly to their special pore morphology and structures, which might be difficult to produce artificially. Moreover, they are a step towards developing environmentally benign routes to obtaining materials of intricate microstructures. Recently, Yang et al. [7] used eggshell membranes as templates to synthesize hierarchically ordered macroporous titania tubes. This paper describes the preparation of a macroporous network of crystalline $LiMn_2O_4$ with eggshell membranes as templates.

T. Sri Devi Kumari · T. Prem Kumar (✉)
Electrochemical Power Systems Division,
Central Electrochemical Research Institute,
Karaikudi, Tamil Nadu, India
e-mail: prem@cecri.res.in

Experimental

Fresh eggs obtained from a local poultry were carefully broken at the blunt end and were emptied of their contents.

The eggshells were repeatedly washed in water, and the inner shell membrane and the limiting membrane were removed with a pair of tweezers. The eggshells with the outer shell membrane were dipped in 2 M HCl to dissolve the calcium carbonate shell. The undissolved outer membrane was washed thoroughly with water and dried in an air oven maintained at 40°C. The dried membranes were then soaked in a methanolic solution of a stoichiometric mixture of $LiNO_3$ and $Mn(NO_3)_2$, the excess solution swabbed with a filter paper, and dried at 110°C. The precursor-laden eggshell membranes were subsequently subjected to heat treatment at 800°C for 5, 10, 15, and 20 h.

The decomposition pattern of the precursor mass was followed by simultaneous thermogravimetric and differential thermal analyses (TA Instruments model SDT Q600) in air from room temperature to 800°C. The heating rate was 5°C/min. Structural characterization of the calcined products was done by a PANalytical model X'per PRO powder X-ray diffractometer with nickel-filtered Cu K_α radiation between scattering angles of 10° and 80° in increments of 0.05°. Morphological features of the products were examined by scanning electron microscopy (Hitachi model S-3000H). The membranes being nonconducting, they were sputtered with gold before scanning electron microscopy (SEM) examination. BET surface area measurements were done by the nitrogen adsorption–desorption method (Micromeritics ASAP 2010). Charge–discharge studies were carried out with coin cells assembled in standard 2032 stainless steel cell hardware. Lithium metal was used as the anode, and a 1-M solution of $LiPF_6$ in ethylene carbonate/diethyl carbonate (EC/DEC) (1:1 *v*/*v*) was used as the electrolyte. The cathode was prepared by blade-coating a slurry of 85 wt.% active material with 10 wt.% conductive carbon black and 5 wt.% PVdF binder in *N*-methyl-2-pyrrolidone on a stainless steel disc and drying the coating overnight at 120°C in an oven. Cell assembly was done in an argon-filled glove box (MBraun MB-120G), which contained less than 2 ppm oxygen and moisture. The cells were cycled between 3.0 and 4.3 V at a 0.1*C* rate on a multi-channel battery tester (Arbin BT2000). Cyclic voltammograms were run on an Autolab potentiostat/galvanostat (Eco Chimie) at a scan rate of 0.100 mV/s between 3.3 and 4.5 V with lithium metal foil serving both as counter and reference electrodes.

Results and discussion

The organic eggshell membranes that line the calcified shell of avian eggs contain collagen types I, V, and X and glycosaminoglycans [8]. The eggshell membrane consists of the outer shell membrane, the inner shell membrane, and the limiting membrane that surrounds the egg white [9]. The outer shell, which can easily be isolated, was used in this study. Here, the outer shell membrane functions as a fugitive phase: upon pyrolysis, it leaves behind an ordered macrostructure of the ceramic phase. The membrane contains functional groups such as amines, amides, and carboxylates, which can help anchor the cations in the precursor solution. Once the fugitive phase is removed by heat treatment, the crystals form a network that assumes a replica of the framework structure of the membrane.

Figure 1 shows the results of thermal analyses on the nitrate precursors, the membrane, and the membrane impregnated with the nitrates. The initial weight loss and the corresponding endotherms in Fig. 1a are related to melting of $Mn(NO_3)_2{\cdot}4H_2O$ (m.p. 37°C) and to loss of superficial water. The decomposition of the nitrate mixture is complex as evident from the number of steps in the thermogravimetry and peaks in the thermogravimetric analysis as well as from the fact the decomposition process sets in much before the melting point of $LiNO_3$ (m.p. 255°C). The final formation of the $LiMn_2O_4$ product appears to be complete above 350°C. In the case of the membrane (Fig. 1b), weight loss is considerable only at temperatures above 200°C, suggesting that water molecules in membrane are strongly bonded to the protein molecules and that it takes higher energies to remove them. In fact, browning of the membrane occurred only above 200°C, which was followed by carbonization over a wide temperature range up to about 550°C, with an endothermic peak around 375°C. In contrast to the thermal behavior of the membrane, it can be seen from Fig. 1c that, in the presence of added salts, the weight loss occurs from room temperature to about 450°C in several steps. It is suggested that the water molecules in the membrane get displaced by the added salts, which get chemically attached to the membrane molecules. The weight loss at the lower temperatures (up to about 150°C) in Fig. 1c suggests a weakening of the water bonding to the membrane. Moreover, $Mn(NO_3)_2{\cdot}4H_2O$ is also known to dehydrate and decompose at temperatures above 100°C. There is also a gradual breakdown of structures and partial carbonization beyond 300°C. The charring process was accompanied by evolution of brown nitrogen dioxide, which became copious as the temperature rose to above 350°C. The final decomposition and product formation occurs around 400°C. A comparison of Fig. 1a, c shows that the final decomposition temperature is higher in the case of the salt-laden membrane, suggesting strong association of metal ions with the protein molecules. Both in Fig. 1a, b, there is an endotherm prior to the final exothermic decomposition. Decomposition reactions are necessarily endothermic because the system must absorb heat from its surroundings to raise its enthalpy to the critical limit of thermodynamic stability, beyond which the decomposition occurs. However, the decomposition of the high-energy molecules to form $LiMn_2O_4$ should, in principle,

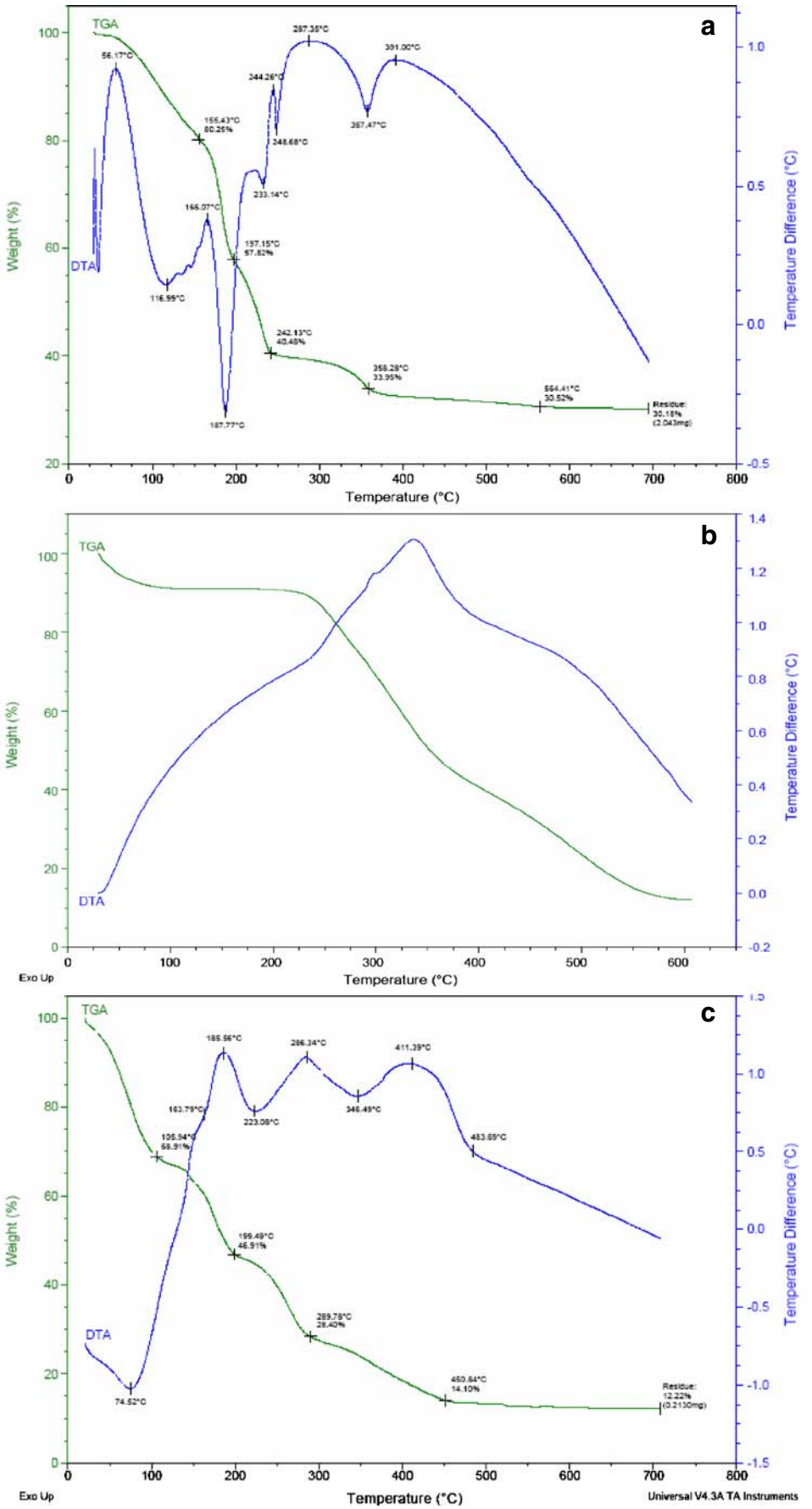

Fig. 1 TG and differential thermal analysis (DTA) profiles of **a** mixture of nitrate precursors; **b** egg membrane; and **c** nitrate-impregnated egg membrane

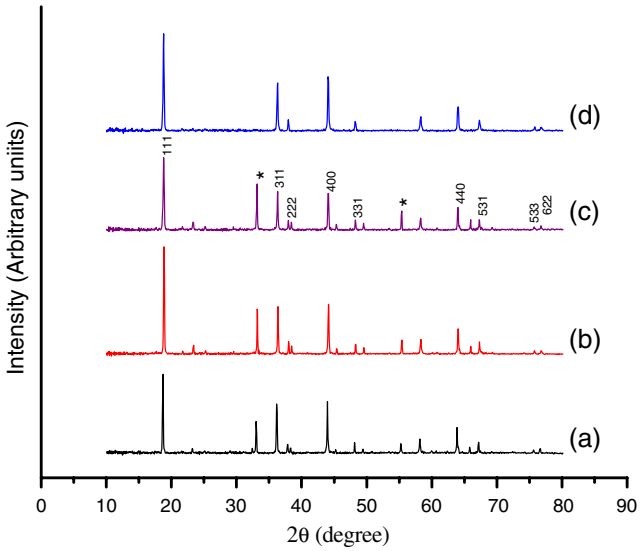

Fig. 2 Powder XRD patterns of $LiMn_2O_4$ calcined at 800°C for **a** 5, **b** 10, **c** 15, and **d** 20 h. Impurity peaks due to Mn_2O_3 are marked with a *star*

be exothermic, a fact reflected by the sudden rise in the differential thermogram towards the exothermic region.

Powder X-ray diffraction (XRD) patterns recorded with the products obtained by calcination at 800°C for 5, 10, 15, and 20 h are shown in Fig. 2. Peaks due to presence of impurities such as Mn_2O_3, especially in products prepared at heating durations, are marked with a star. The diffraction patterns correspond to the cubic spinel structure in *Fd3m* space group of $LiMn_2O_4$. The values of the lattice parameter *a* calculated from the XRD data are 8.113, 8.139, 8.157, and 8.163 Å for samples calcined for 5, 10, 15, and 20 h, respectively (Table 1). The values are less than the 8.244 Å reported for $LiMn_2O_4$ synthesized by a solid-state method at 750°C [10]. The lattice parameter for the cubic spinel is generally believed to depend on the average oxidation state of manganese. Because of the greater stability of Mn^{4+} ions at low temperatures, a significant fraction of the manganese ions in insufficiently calcined spinels is present in the 4+ state [11]. Therefore, the presence of larger amounts of the smaller Mn^{4+} ions (Mn^{4+}, 0.60 Å; Mn^{3+}, 0.68 Å [12]) in the incompletely calcined samples should lead to diminished values of *a*. With the replacement of part of the Mn^{4+} ions with Mn^{3+} ions at the higher temperatures, the cubic lattice parameter also increases.

The BET surface area of a typical sample (800°C, 10 h) was 2.53 m^2/g. An SEM image of the membrane template presented in Fig. 3a shows a macroporous network of interwoven and coalescing membrane fibers with diameters ranging from 0.5 to 2 μm. Figure 3b is an SEM image of the $LiMn_2O_4$ product obtained by a 10-h calcination at 800°C. Figure 3c shows the network structure at a higher magnification. It can be seen that the $LiMn_2O_4$ product is obtained as well-developed crystals of uniform size of about 600 nm. A comparison of Fig. 3a, b shows that there is a considerable shrinkage in the network structure from the eggshell membrane (5–20 μm) to that of the product (0.5–2 μm). The shrinkage is attributed to the loss of moisture and other volatiles from the membrane during the initial stages of pyrolysis.

The galvanostatic cycling performances of the macroporous $LiMn_2O_4$ products calcined at 800°C for different durations are shown in Fig. 4. The first-cycle capacities observed with these materials were 101.9, 116.8, 117.3, and 115.5 mAh/g for calcination durations of 5, 10, 15, and 20 h, respectively. The first-cycle capacity values are generally in agreement with the fact that the amount of Mn^{3+} ions in the sample increases with heat treatment [11]. The poor cycling behavior of the 5-h heated sample also reflects the poor crystallinity of the product. However, the drop in capacity for the sample calcined for 20 h must be attributed to loss of lithium upon prolonged heating. Figure 4 shows that the best performing electrode is the one calcined at 800°C for 10 h. This material could sustain 83 cycles before its capacity retention reached 80%.

Cyclic voltammetric profiles of the product obtained by 10-h calcination at 800°C (Fig. 5) shows two redox peaks at 4.09 and 4.22 V (and the corresponding ones on the reverse scan at 4.03 and 3.82 V) that are characteristic of crystalline $LiMn_2O_4$ [13]. According to Ohzuku et al. [14] and Liu et al. [15], the peaks arise from two co-existing cubic phases during the reversible lithium intercalation processes, viz., $LiMn_2O_4 \leftrightarrow Li_{0.5}Mn_2O_4$ and $Li_{0.5}Mn_2O_4 \leftrightarrow \lambda\text{-}MnO_2$. The occurrence of the two peaks is a manifestation of the difference between the energies of lithium intercalation for

Table 1 Lattice parameters of $LiMn_2O_4$ prepared by 800°C-calcination for different durations

Duration of calcination (h)	Lattice parameter *a* (Å)	Unit cell volume ($Å^3$)
5	8.113 (±0.004)	534.0
10	8.139 (±0.005)	539.2
15	8.157 (±0.004)	542.7
20	8.163 (±0.003)	543.9

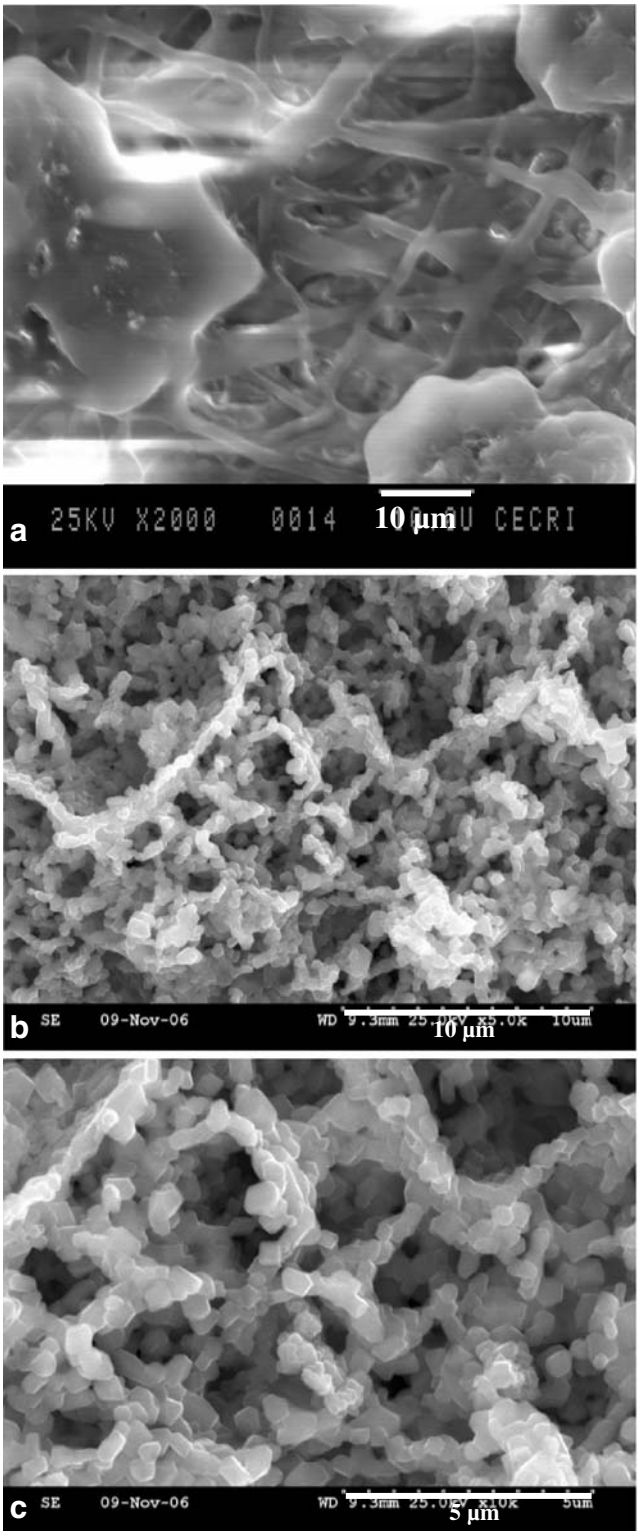

Fig. 3 SEM images of **a** dry egg membrane, **b**, **c** $LiMn_2O_4$ products obtained by calcination at 800°C for 10 h at two magnifications

values of x below and above 0.5 in $Li_xMn_2O_4$ [14, 16–19]. The energy difference is attributed to lithium ion ordering that must precede the greater occupation of the 8*a* tetrahedral sites in the spinel [14, 16–19].

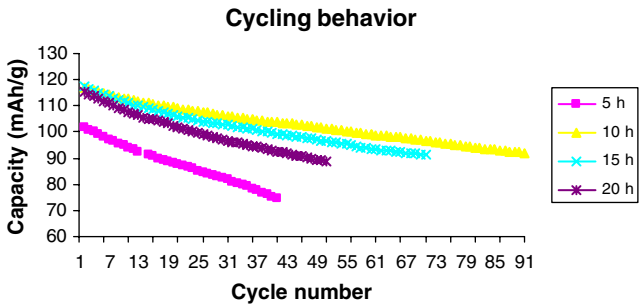

Fig. 4 Cycling behavior of macroporous $LiMn_2O_4$ products obtained by calcination at 800°C for 5, 10, 15, and 20 h

Conclusions

Preparation of a macroporous network of crystalline $LiMn_2O_4$ by a replica method using avian eggshell membrane as a template is demonstrated. Precursor salts get chemically attached to the fugitive membrane phase, the removal of which yields products that replicate the original structure. Dehydration accompanying the water loss during heat treatment shrinks the membrane considerably. The final products were well-formed flake-like crystals of average size 600 nm distributed in a network whose average pore size was 2–4 µm. At a 0.1*C* rate, a $LiMn_2O_4$ sample obtained by a 10-h calcination at 800°C gave a first-cycle capacity of 117 mAh/g between 3.0 and 4.3 V and sustained 83 cycles before reaching 80% capacity retention. The study demonstrates the use of avian egg membrane as an inexpensive and easily available biological membrane for the preparation of macroporous $LiMn_2O_4$.

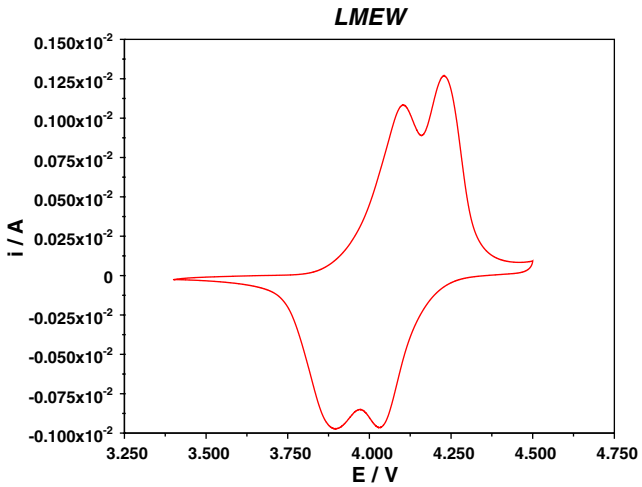

Fig. 5 Cyclic voltammogram of $LiMn_2O_4$ obtained by 10-h calcination at 800°C. Scan rate, 0.100 mV/s

Acknowledgments Financial support for this work by the Department of Science and Technology, Government of India under its SERC scheme is gratefully acknowledged. TSDK thanks her project leader, Dr. B. Emmanuel, for his interest in this work.

References

1. Davis SA, Burkett SL, Mendelson NH, Mann S (1997) Nature 385:420
2. Zhang B, Davis SA, Mann S (2002) Chem Mater 14:1369
3. Colombo P (2006) Philos Trans Roy Soc A 364:109–24
4. Studart AR, Gonzenbach UT, Tervoort E, Gauckler LJ (2006) J Am Ceram Soc 89:1771
5. Lee YJ, Lee JS, Park YS, Yon KB (2001) Adv Mater 13:1259
6. Shin Y, Liu J, Chang JH, Nie Z, Exarhos GJ (2001) Adv Mater 13:728
7. Yang D, Qi L, Ma J (2002) Adv Mater 14:1543
8. Dennis JE, Carrino DA, Yamashita K, Caplan AI (2000) Matrix Biol 19:683
9. Hincke MT, Gautron J, Panheleux M, Garcia-Ruiz J, McKee MD, Nys Y (2000) Matrix Biol 19:443
10. Gao Y, Dahn JR (1996) J Electrochem Soc 143:100
11. Masquelier C, Tabuchi M, Ado K, Kanno R, Kobayashi Y, Maki Y, Nakamura O, Goodenough JB (1996) J Solid State Chem 123:255
12. Borchardt-Ott W (1993) Crystallography. Springer, New York
13. Tarascon JM, Wang E, Shokoohi FK, McKinnon WR, Colson S (1991) J Electrochem Soc 138:2859
14. Ohzuku T, Kitagawa M, Hirai T (1990) J Electrochem Soc 137:769
15. Liu W, Farrington GC, Chaput F, Dunn B (1996) J Electrochem Soc 143:879
16. Han YS, Kim HG (2000) J Power Sources 88:161
17. Roussouw MH, de Kock A, de Picciotto LA, Thackeray MM, David WIF, Ibberson RM (1990) Mater Res Bull 25:173
18. Tarascon JM, Coowar F, Amatucci GG, Shokoohi FK, Guyomard D (1995) J Power Sources 54:103
19. Hwang BJ, Santhanam R, Liu DG (2001) J Power Sources 97–98:443